

Investigating the effect of PBH, Dark matter - baryon and Dark matter - Dark Energy interaction on EDGES in 21cm Signal

Ashadul Halder*

*Department of Physics, St. Xavier's College, 30,
Mother Teresa Sarani, Kolkata-700016, India.*

Madhurima Pandey†

*Astroparticle Physics and Cosmology Division,
Saha Institute of Nuclear Physics, HBNI,
1/AF Bidhannagar, Kolkata 700064, India*

(Dated: February 28, 2025)

Abstract

21cm radio signal has emerged as an important probe in investigating the Dark Age of the Universe (recombination to reionization). In the current analysis, we explore the combined effect of baryon - dark matter interaction, primordial black holes (PBH) on the 21cm brightness temperature. The variation of brightness temperature shows remarkable dependence on dark matter mass (m_χ) and the baryon - dark matter cross-section (σ_0). We address a bound in the m_χ - σ_0 space in presence of PBH in the framework of three different Interacting Dark Energy (IDE) models of the Universe. The limits are estimated based on the observed excess (-500^{+200}_{-500} mK) of 21cm brightness temperature by EDGES experiment. Eventually, a bound on PBH mass is also estimated for different values of dark matter mass and the IDE model coupling parameters and the compatibility of the IDE model constraints in the estimated bounds are also addressed.

Keywords: 21 cm; dark energy; dark matter; primordial black hole

* ashadul.halder@gmail.com

† madhurima.pandey@saha.ac.in

I. INTRODUCTION

The 21cm cosmology is turning out to be a promising tool in understanding the dynamics of the early Universe. The redshifted signature of the 21cm neutral hydrogen spectra opens up a new window to understand the process of reionization and the factors in the early Universe influencing the same. Thus study of the 21cm line in reionization era helps in understanding several cosmological and astrophysical processes that might have contributed to the physics of the early Universe.

The 21cm (~ 1.42 GHz) hyperfine spectra is originated by the transition between two spin states ($s=0$ and 1) of the electron of H atoms and its nucleus. The hydrogen occupies around 75% of the entire baryonic mass of the Universe. The corresponding spin temperature indicates the population of hydrogen atom with different energy states. The “Experiment to Detect the Global Epoch of Reionization Signature” (EDGES) [1] reported 21cm absorption spectra at the cosmic dawn era ($14 < z < 20$) and predicted the 21cm brightness temperature to be -500^{+200}_{-500} mK with 99% confidence level (C.L.).

The 21 cm brightness temperature T_{21} depends on $T_s - T_\gamma$, where T_s is the spin temperature and the T_γ is the background temperature (CMB temperature). The observed additional cooling of T_{21} by EDGES experiment can be realised by either enhancing the background temperature T_γ or by lowering the matter temperature which is equal to T_s at that epoch. Dark matter interactions such as the processes of dark matter - baryon scattering, dark matter annihilation or decay can inject energy into the background resulting in the rise in background temperature. There can be other processes, which can induce the larger than expected difference of T_s and T_γ . The evaporation of Primordial Black Holes can well be such a candidate to inject more energy to the system by the process of its evaporation.

Primordial Black Holes (PBH) [2–5] are believed to be formed during the radiation dominated era. It forms due to the collapse of the overdensity region characterized by the size of the region which should be greater than the Jeans length R_j , $R_j = \sqrt{\frac{1}{3G\rho}}$. Also the condition of the PBH formation is $\delta_{\min} \leq \delta \leq \delta_{\max}$, where δ is the density contrast. The maximum and minimum density contrast δ_{\max} and δ_{\min} respectively are governed by the value of $\delta\rho$, where the density $\rho = \rho_c + \delta\rho$, where ρ_c is the critical density for collapse. The δ_{\min} is the threshold of PBH formation. In the work of [6], the masses of the PBHs are considered $\geq 10^{15}$ g. But in the current work we investigate the 21cm signal with the PBH

masses $10^{13} \leq \mathcal{M}_{\text{BH}} \leq 10^{14}$ g as focused in the work of [7].

In this work we consider the possible influence on 21cm EDGES signal of the factors namely baryon - Dark Matter scattering, possible Dark Matter - Dark Energy interaction and the evaporation of primordial black holes or PBH [6–10] simultaneously in the epoch of ignition of first star. In the present work, the dark matter baryon interaction cross-section ($\bar{\sigma}$) is parameterized as $\bar{\sigma} = \sigma_0 v^{-4}$ [11]. The heating effect by the PBHs are considered here in the form of Hawking Radiation only. The effect of DM - DE interaction only is considering the IDE models given in Li *et al.* [12]. The DM - DE interaction is later addressed by Mukhopadhyay *et al.* [13] where the latter incorporated both the baryon - DM scattering and DM - DE interaction in the same framework of 21cm temperature evolution. The Dark Matter - Dark Energy interaction can also influence T_s and thus T_{21} . In fact, the influence of DM - DE interaction is discussed in [12, 13] with three interacting Dark Energy (IDE model).

The paper is organized as follows. In Section II, we address the interaction between Dark Matter and Dark Energy and its effect in cosmic evolution. Section III deals with the energy injection by the PBHs in the form of Hawking radiation. In Section IV and Section V, the thermal evolutions of the Universe are described. Corresponding results with their demonstrative plots are furnished in Section VI. Finally in Section VII, concluding remarks are given.

II. DARK MATTER DARK ENERGY INTERACTION

The DM - DE interaction may have a profound effect in the Universal dynamics and hence on the optical depth and spin temperature of the 21cm transition. In standard cosmological model, the density parameters of dark matter (Ω_χ) and dark energy (Ω_{de}) are assumed to be evolved as $\Omega_{\chi,0}(1+z)^3$ and $\Omega_{\text{de},0}(1+z)^{3(1+\omega)}$ where, $\Omega_{\chi,0}$ and $\Omega_{\text{de},0}$ are the density parameters at $z = 0$ and ω is the equation of state parameter of dark energy. However, as the interaction between dark matter and dark energy is taken into account, the said evolution of dark matter and dark energy are no longer valid and take the forms [12],

$$(1+z)H(z)\frac{d\rho_\chi}{dz} - 3H(z)\rho_\chi = -\mathcal{Q} \quad (1)$$

$$(1+z)H(z)\frac{d\rho_{\text{de}}}{dz} - 3H(z)(1+\omega)\rho_{\text{de}} = \mathcal{Q} \quad (2)$$

Model	\mathcal{Q}	EOS of Dark Energy	Constraints
I	$3 \lambda H(z) \rho_{\text{de}}$	$\omega < -1$	$\lambda < -2\omega\Omega_\chi$
II	$3 \lambda H(z) \rho_\chi$	$\omega < -1$	$0 < \lambda < -\omega/4$
III	$3 \lambda H(z) (\rho_{\text{de}} + \rho_\chi)$	$\omega < -1$	$0 < \lambda < -\omega/4$

TABLE I. Stability conditions of the model parameters for different IDE models

Model	ω	λ	H_0
$3\lambda H \rho_{\text{de}}$	$-1.088^{+0.0651}_{-0.0448}$	$0.05219^{+0.0349}_{-0.0355}$	$68.35^{+1.47}_{-1.46}$
$3\lambda H \rho_\chi$	$-1.1041^{+0.0467}_{-0.0292}$	$0.0007127^{+0.000256}_{-0.000633}$	$68.91^{+0.875}_{-0.997}$
$3\lambda H (\rho_{\text{de}} + \rho_\chi)$	$-1.105^{+0.0468}_{-0.0288}$	$0.000735^{+0.000254}_{-0.000679}$	$68.88^{+0.854}_{-0.97}$

TABLE II. Constraints of the different IDE models

where \mathcal{Q} denotes the energy transfer between dark matter and dark energy during the interaction. In the present work we consider three benchmark models in order to investigate the effect of DM-DE interaction in the brightness temperature. The energy transfer expression of those benchmark models are described below [14–17].

$$\begin{aligned}
\text{Model-I} \quad \mathcal{Q} &= 3\lambda H(z) \rho_{\text{de}} \\
\text{Model-II} \quad \mathcal{Q} &= 3\lambda H(z) \rho_\chi \\
\text{Model-III} \quad \mathcal{Q} &= 3\lambda H(z) (\rho_{\text{de}} + \rho_\chi)
\end{aligned}$$

Here, λ the interaction coupling parameter, which determines the strength of the interaction. The limiting conditions for the individual models are described in Table I. Several phenomenological studies have been carried out with observational data of PLANCK, Supernova Ia (SNIa) Baryon Acoustic Oscillation (BAO) [16–23] yielding the constraints for different models (in Table II).

III. EFFECT OF PRIMORDIAL BLACK HOLE

The energy injection of PBHs in the form Hawking radiation [24] can be a possible source for heating up of the Inter Galactic Medium (IGM) before the reionization. The work of Clark *et al.* [6] shows that, in 21cm scenario, the Hawking radiation is equally significant as that of the DM decay.

The mass evaporation rate due to Hawking radiation can be expressed as

$$\frac{d\mathcal{M}_{\text{BH}}}{dt} \approx -5.34 \times 10^{25} \left(\sum_i \mathcal{F}_i \right) \mathcal{M}_{\text{BH}}^{-2} \text{ g/sec} \quad (3)$$

where, \mathcal{M}_{BH} is the mass of black hole and $\sum_i \mathcal{F}_i$ is the sum over all fraction of evaporation, defined as [24],

$$\begin{aligned} \sum_i \mathcal{F}_i = & 1.569 + 0.569 \exp\left(-\frac{0.0234}{T_{\text{BH}}}\right) + 3.414 \exp\left(-\frac{0.066}{T_{\text{BH}}}\right) \\ & + 1.707 \exp\left(-\frac{0.11}{T_{\text{BH}}}\right) + 0.569 \exp\left(-\frac{0.394}{T_{\text{BH}}}\right) \\ & + 1.707 \exp\left(-\frac{0.413}{T_{\text{BH}}}\right) + 1.707 \exp\left(-\frac{1.17}{T_{\text{BH}}}\right) \\ & + 1.707 \exp\left(-\frac{22}{T_{\text{BH}}}\right) + 0.963 \exp\left(-\frac{0.1}{T_{\text{BH}}}\right) \end{aligned} \quad (4)$$

In the above expression, T_{BH} represents the temperature of the black hole given by, $T_{\text{BH}} = 1.05753 \times (\mathcal{M}_{\text{BH}}/10^{13} \text{g})$. The energy emission in the form of photons and electrons are only considered in the current work as only those can interact with the IGM [6]. In contrast, the contribution of neutrinos and other species in gas heating is negligible. The energy injection rate per unit volume due to PBHs is given by [6],

$$\left. \frac{dE}{dV dt} \right|_{\text{BH}} = \sum_{i=\gamma, e^\pm} \mathcal{F}_i \frac{d\mathcal{M}_{\text{BH}}}{dt} n_{\text{BH}}(z) \quad (5)$$

$$\left. \frac{dE}{dV dt} \right|_{\text{BH}} = \sum_{i=\gamma, e^\pm} \mathcal{F}_i(\mathcal{M}_{\text{BH}}) \frac{1}{\mathcal{M}_{\text{BH}}} \frac{d\mathcal{M}_{\text{BH}}}{dt} \rho_{c,0} \Omega_{\text{BH}} (1+z)^3, \quad (6)$$

where, $n_{\text{BH}}(z)$ is the number density of black hole at redshift z . The black hole number density ($n_{\text{BH}}(z)$) can be expressed as a function of cosmological redshift (z) and initial mass fraction of primordial black holes (β_{BH}), given by,

$$\begin{aligned} n_{\text{BH}}(z) = & \beta_{\text{BH}} \left(\frac{1+z}{1+z_{\text{eq}}} \right)^3 \frac{\rho_{c,\text{eq}}}{\mathcal{M}_{\text{BH},i}} \left(\frac{\mathcal{M}_{\text{H,eq}}}{\mathcal{M}_{\text{H}}} \right)^{1/2} \left(\frac{g_\star^i}{g_\star^{\text{eq}}} \right)^{1/12} \\ \approx & 1.46 \times 10^{-4} \beta_{\text{BH}} (1+z)^3 \left(\frac{\mathcal{M}_{\text{BH},i}}{\text{g}} \right)^{-3/2} \text{ cm}^{-3}. \end{aligned} \quad (7)$$

IV. TEMPERATURE EVOLUTION

The thermal evolution of the Universe is studied by evolving the baryon temperature (T_b) and the dark matter temperature (T_χ) with redshift z . As mentioned we have considered

three effects namely baryon - DM scattering, DM - DE interaction and evaporation of PBH in temperature evolution of baryon and Dark Matter and finally compute the 21cm brightness temperature (T_{21}). The effect of baryon - Dark Matter scattering has earlier been addressed in the context of 21cm signal by Muñoz *et al.* [11]. More recently the effect of DM - DE interaction is also included along with baryon - DM scattering by Mukhopadhyay *et al.* [13]. In the present work, the effects of DM-DE interaction and the PBHs are incorporated in the evolution equations of T_χ and T_b following the procedure given in [13, 25],

$$(1+z)\frac{dT_\chi}{dz} = 2T_\chi - \frac{2\dot{Q}_\chi}{3H(z)} - \frac{1}{n_\chi} \frac{2\mathcal{Q}}{3H(z)}, \quad (8)$$

$$(1+z)\frac{dT_b}{dz} = 2T_b + \frac{\Gamma_c}{H(z)}(T_b - T_\gamma) - \frac{2\dot{Q}_b}{3H(z)} - \mathcal{J}_{\text{BH}}. \quad (9)$$

where, the last term of Eqn. 8 indicates the effects of dark matter-dark energy interaction (see Section II) and the last term of Eq. 9 ($\mathcal{J}_{\text{BH}} = \frac{2}{3k_B H(z)} \frac{K_{\text{BH}}}{1+f_{\text{He}}+x_e}$) represents the contribution of PBHs in the form of Hawking radiation [7]. In the above evolution equations, T_γ ($T_\gamma = 2.725(1+z)$ K) is the CMB temperature and Γ_c ($\Gamma_c = \frac{8\sigma_T a_r T_\gamma^4 x_e}{3(1+f_{\text{He}}+x_e)m_e c}$) describes the Compton interaction rate (σ_T and a_r are the Thomson scattering cross-section and radiation constant respectively). f_{He} and x_e are the fractional abundance of He and electron respectively. The heating rates \dot{Q}_b and \dot{Q}_χ are estimated as described in the work of Muñoz *et al.* [11] (b and χ are indicating baryon and DM respectively) which depends on the drag term $V_{\chi b}$.

The free electron abundance x_e is an important quantity in estimating thermal evolution. It also influences T_b and T_γ simultaneously. This evolution is given by,

$$\frac{dx_e}{dz} = \frac{1}{(1+z)H(z)} [I_{\text{Re}}(z) - I_{\text{Ion}}(z) - I_{\text{BH}}(z)], \quad (10)$$

where $I_{\text{Re}}(z)$ and $I_{\text{Ion}}(z)$ are the standard recombination rate and standard ionization rate respectively. The combined effect of these two coefficients is described as,

$$I_{\text{Re}}(z) - I_s(z) = C_P \left(n_H \alpha_B x_e^2 - 4(1-x_e)\beta_B e^{-\frac{3E_0}{4k_B T_\gamma}} \right). \quad (11)$$

In Eq. 11, C_P represents the Peebles C factor [26, 27], α_B and β_B are the case B recombination and ionization coefficients respectively.

The expression of α_B (in m^3s^{-1}) as a function of temperature, can be obtained by data fitting as obtained in the work of Pequignot *et al.* [28]. The fitted expression of α_B with parameters $a = 4.309$, $b = -0.6166$, $c = 0.6703$, $d = 0.5300$, $F = 1.14$ is given by [10, 28],

$$\alpha_B = 10^{-19} F \left(\frac{at^b}{1+ct^d} \right), \quad (12)$$

where, t represents the temperature in 10^4K [28–30]. The expression for photoionization coefficient (β_B) (in term of α_B) as written in [10, 30],

$$\beta_B = \alpha_B \left(\frac{2\pi\mu_e k_B T_\gamma}{h^2} \right)^{3/2} \exp \left(-\frac{h\nu_{2s}}{k_B T_\gamma} \right), \quad (13)$$

where, μ_e is the reduced mass of electron-proton system and ν_{2s} is the frequency for $2s \rightarrow 1s$ transition. The Peebles C factor reads as [27],

$$C_P = \frac{\frac{3}{4}R_{Ly\alpha} + \frac{1}{4}\Lambda_{2s1s}}{\beta_B + \frac{3}{4}R_{Ly\alpha} + \frac{1}{4}\Lambda_{2s,1s}}. \quad (14)$$

In the above, $R_{Ly\alpha}$ represents the rate of escape of $Ly\alpha$ photons ($R_{Ly\alpha} = 8\pi H / (3n_H(1 - x_e)\lambda_{Ly\alpha}^3)$) and $\Lambda_{2s,1s} \approx 8.22\text{s}^{-1}$ [27].

$$I_{BH} = \chi_i f \frac{1}{n_b} \frac{1}{E_0} \times \frac{dE}{dV dt} \Big|_{BH}, \quad (15)$$

$$K_{BH} = \chi_h f \frac{1}{n_b} \times \frac{dE}{dV dt} \Big|_{BH}. \quad (16)$$

where $E_0 = 13.6\text{ eV}$, $f = 0.1$ [31], $\chi_i = (1 - x_e)/3$ and $\chi_h = (1 + 2x_e)/3$ [7, 32]

The relative velocity between matter and dark matter ($V_{\chi b} \equiv V_\chi - V_b$) emerges as an important consequence with redshift, as discussed in [11]. The evolution of the drag term is given by the equation

$$\frac{dV_{\chi b}}{dz} = \frac{V_{\chi b}}{1+z} + \frac{D(V_{\chi b})}{(1+z)H(z)}, \quad (17)$$

with initial condition $V_{\chi b} = 29\text{ km/s}$. In the above equation, the drag term $D(V_{\chi b})$ is defined as,

$$D(V_{\chi b}) = \frac{d(V_{\chi b})}{dt} = \frac{\rho_m \sigma_0}{m_b + m_\chi} \frac{1}{V_{\chi b}^2} F(r) \quad (18)$$

In the above, $F(r) = \text{erf}(r/\sqrt{2}) - \sqrt{2/\pi} r e^{-r^2/2}$, where r is defined as $r = V_{\chi b}/u_{th}$ and $u_{th} = \sqrt{T_b/m_b + T_\chi/m_\chi}$ is the variance of the thermal relative motion of baryon - Dark Matter fluid and σ_0 is the baryon - Dark Matter scattering cross-section while σ_{41} is the same in units of 10^{-41}cm^2 .

V. 21CM COSMOLOGY

As mentioned earlier, the 21cm line is originated due to the transition of electron between the triplet and singlet states of the hydrogen atom (spin 0 and spin 1). The intensity of the 21cm line is represented by the brightness temperature (T_{21}) which depends on optical

depth (τ) and hence the Hubble parameter ($H(z)$). The variation of brightness temperature of the 21cm hydrogen spectra with redshift (z) is given by,

$$T_{21} = \frac{T_s - T_\gamma}{1 + z} (1 - e^{-\tau}) \cong \frac{T_s - T_\gamma}{1 + z} \tau, \quad (19)$$

where, T_s and T_γ are spin temperature and CMB temperature respectively at redshift z . As the numerical values of τ for different z are very small, we use the approximation in the above equation (Eqn. 19). The optical depth (τ) is given by,

$$\tau = \frac{3}{32\pi} \frac{T_\star}{T_s} n_{\text{HI}} \lambda_{21}^3 \frac{A_{10}}{H(z) + (1 + z)\delta_r v_r} \quad (20)$$

where, λ_{21} (≈ 21 cm) is the 21cm wavelength, T_\star ($= hc/k_B \lambda_{21} = 0.068$ K) is the 21cm temperature, A_{10} ($= 2.85 \times 10^{-15} \text{ s}^{-1}$) is the Einstein coefficient [33].

The spin temperature T_s basically describes the ratio of excited (n_1) to ground state (n_0) neutral hydrogen number density, given by $n_1/n_0 = 3 \exp -T_\star/T_s$. In equilibrium T_s is given by

$$T_s = \frac{T_\gamma + y_c T_b + y_{\text{Ly}\alpha} T_{\text{Ly}\alpha}}{1 + y_c + y_{\text{Ly}\alpha}}, \quad (21)$$

where, $y_{\text{Ly}\alpha}$ represents the Wouthuysen-Field effect in T_s . The quantities y_c , and $T_{\text{Ly}\alpha}$ are the collisional coupling parameters and the Lyman- α background temperature respectively [6], y_c and $y_{\text{Ly}\alpha}$ are defined as $y_c = \frac{C_{10} T_\star}{A_{10} T_b}$ and $y_{\text{Ly}\alpha} = \frac{P_{10} T_\star}{A_{10} T_{\text{Ly}\alpha}} e^{0.3 \times (1+z)^{1/2} T_b^{-2/3} \left(1 + \frac{0.4}{T_b}\right)^{-1}}$ [7, 34–36]. C_{10} is the collision deexcitation rate and $P_{10} \approx 1.3 \times 10^{-21} S_\alpha J_{-21} \text{ s}^{-1}$ is the deexcitation rate due to Lyman- α , where S_α and J_{-21} are the spectral distraction factor [37] and the Lyman- α background intensity [38] respectively.

VI. CALCULATION AND RESULTS

In this work, we explore the significance of 21cm hydrogen line in reionization era by considering the possible simultaneous effects of Hawking radiation from PBHs along with the DM-baryon interaction. In doing this, we numerically solve seven coupled equations, (Eqs. 1, 2, 3, 8, 9, 10 and 17) simultaneously. In Fig. 1, the evolution of baryon temperature (T_b), CMB temperature (T_γ) and the corresponding spin temperature (T_s) are described graphically. The solid red line describes the baryon temperature (T_b) and spin temperature (T_s , red dashed line) variations in presence of PBHs of mass $\mathcal{M}_{\text{BH}} = 10^{14}$ gram and dark matter mass $m_\chi = 0.1$ GeV, where the IDE Model I (model parameters are chosen from

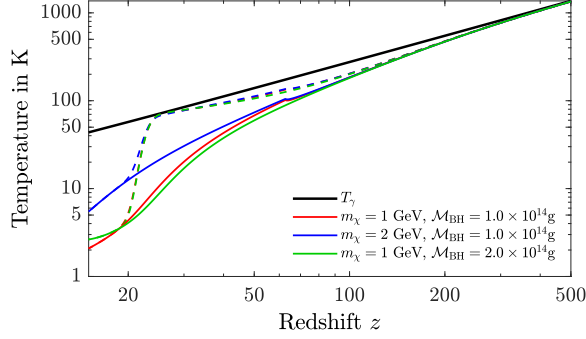


FIG. 1. The variation of baryon temperature T_b , background temperature T_γ , spin temperature T_s with redshift z . The black solid line represents the variation of T_γ and the coloured solid lines and dashed lines corresponds to the variations of T_b and T_s respectively for different sets of dark matter mass m_χ and PBH mass \mathcal{M}_{BH} . Note that for T_s , the plots for all three sets almost coincide. For both T_b and T_s , the computation are made with Model I (Table I and II) only.

Table. II) is considered. The blue and green solid and dashed lines are for the same with $m_\chi = 2 \text{ GeV}$, $\mathcal{M}_{\text{BH}} = 10^{14} \text{ g}$ and $m_\chi = 1 \text{ GeV}$, $\mathcal{M}_{\text{BH}} = 10^{14} \text{ g}$ respectively. In all the cases however Model I for DM - DE interaction is used. It can also be seen that, while the variation of T_b with z differ for different choices of m_χ and \mathcal{M}_{BH} below $z \sim 100$. Such variations for T_s are barely observed except very mildly around $z \sim 20$.

In Fig. 2 we demonstrate how the 21cm brightness temperature T_{21} is affected for different dark matter mass m_χ and baryon - Dark Matter scattering (different values of σ_{41}). We plot in Fig. 2 the variations of T_{21} with z for different values of m_χ for a fixed value of $\sigma_{41} = 1$ (Fig. 2a) and for different values of σ_{41} for a fixed value of $m_\chi = 1 \text{ GeV}$ (Fig. 2b). For both the cases, the PBH mass is fixed at $\mathcal{M}_{\text{BH}} = 1.5 \times 10^{14} \text{ g}$. It appears from Fig. 2b that higher values of scattering cross-section favours lowering of T_{21} .

In presence of the DM - DE interaction, the Dark Matter and Dark Energy density parameters evolve non-linearly with redshift z . As a consequence, a remarkable variations in the evolution of Hubble parameter H is manifested (see Fig. 3). In Fig. 3, the variation of Hubble parameter as a dimensionless quantity $H(z)/H_0$ (H_0 is the current value of Hubble parameter) is shown with redshift z . The left panel of Fig. 3 (Fig. 3a, 3c and 3e) are shows the variation of Hubble parameter with redshift z for different values of IDE coupling parameter

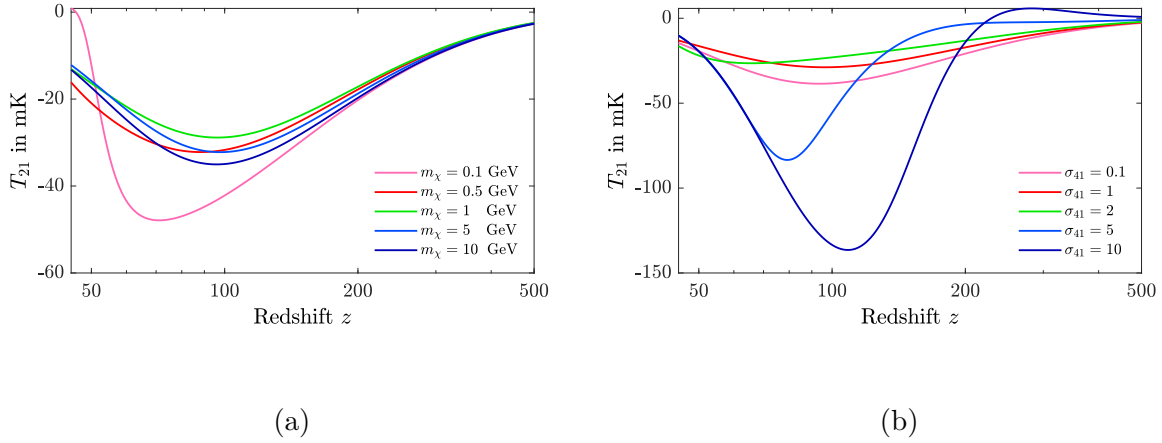


FIG. 2. Variation of brightness temperature (T_{21}) with redshift (z) (a) for different values of m_χ (0.1 GeV, 0.5 GeV, 1 GeV, 5 GeV and 10 GeV) in presence of PBH mass $\mathcal{M}_{\text{BH}} = 1.5 \times 10^{14}$ gram and $\sigma_{41} = 1$. The Fig. 2(b) describes the variation with different values of σ_{41} ($\sigma_{41} = 0.1, 1, 2, 5, 10$) where the PBH mass $\mathcal{M}_{\text{BH}} = 10^{14}$ gram and $m_\chi = 1$ are considered.

λ , where the different values of λ are represented by different colors (cyan to magenta, see colour-bars). On the other hand, Fig. 3b, 3d and 3f (right panel of Fig. 3) shows the variations of $H(z)/H_0$ with λ and the equation of state parameter (ω) simultaneously. The plots (Fig. 3a, 3c and 3e (left panel of Fig. 3) correspond to Model I, II and III respectively of DM - DE interaction. In the right panel of Fig. 3, the plots the Fig. 3b, 3d and 3f also correspond to Model I, II and III respectively. In all the three plots of the left panel of Fig. 3 (for model I, II and III), the values of the equation of state parameter ω are adopted from Table II and they are keep fixed for the corresponding models. In each of the plots of Fig. 3, the dashed black line represents the Λ CDM case ($\lambda = 0$). Analysing all the furnished figures in Fig. 3, one can conclude that, the evolution of Hubble parameter is almost identical in the case of Model II and Model III where the variations are mostly depend on λ (see Fig. 3d and 3e, the dependence on ω is minimal) and the variation is almost linear in nature (see Fig. 3c and 3d). Nonetheless, very small difference can be observed between the Model II and Model III in Fig. 3d and 3e (also between Fig. 3c and 3d). In contrast, in case of Model I, both the parameters, λ and ω are equally significant in the Hubble parameter evolution (see Fig. 3b). From Fig. 3a, it can be observed that, initially $H(z)/H_0$ decreases gradually with increasing coupling parameter λ . But later (for higher values of λ) $H(z)/H_0$ suffers rapid

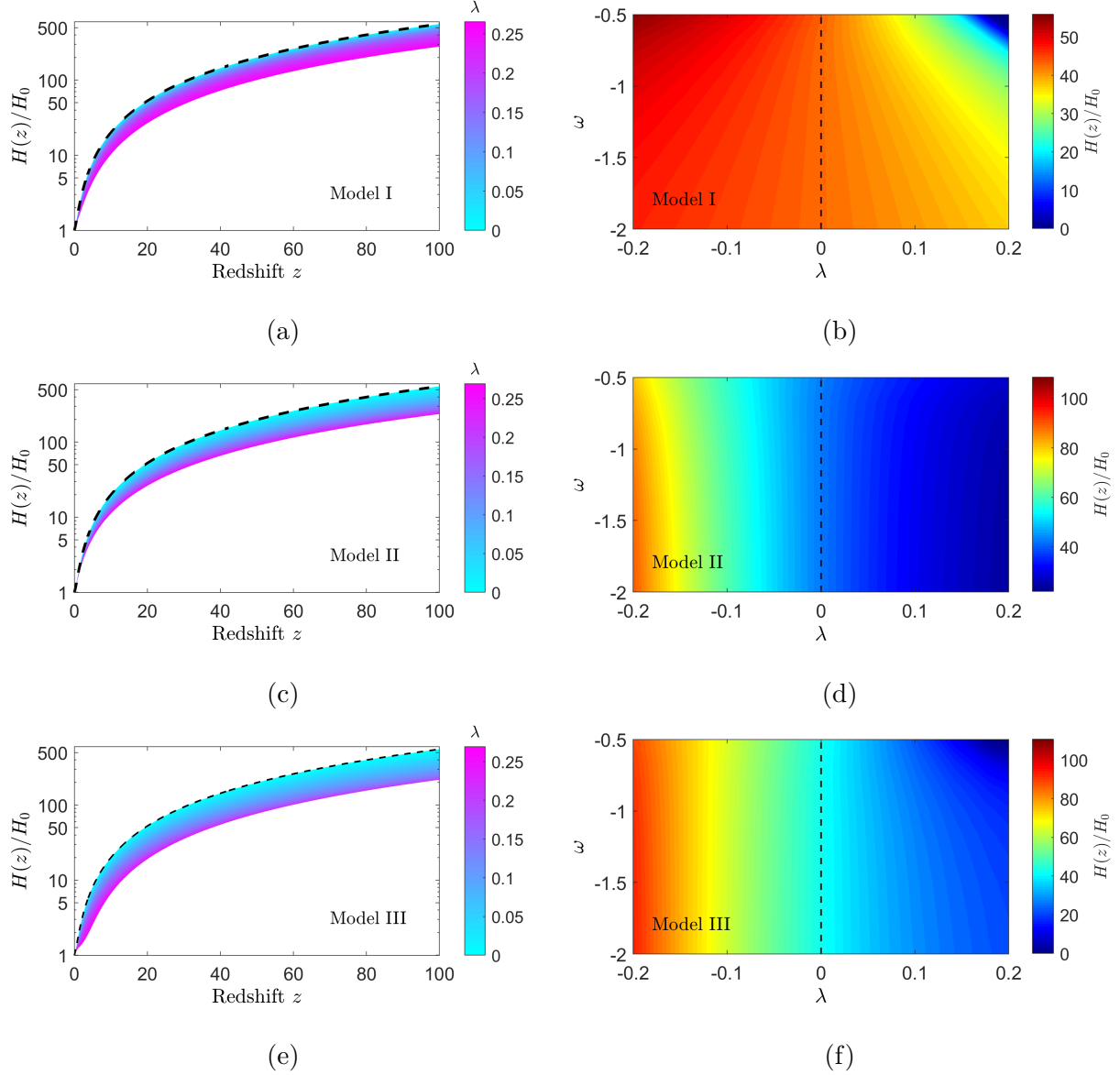


FIG. 3. Evolution of hubble parameter ($H(z)$) for different models (Model I, Model II and Model III) with different values of coupling parameters λ . The left-hand figures (Fig. 3a, 3c and 3e) are indicating the $H(z)$ evolution for different values of λ where the other parameters (ω and H_0) are chosen from Table II). The right-hand figures (Fig. 3b, Fig. 3d and Fig. 3f) are describing the variation of $H(z)$ with both parameter λ and ω (keeping H_0 fixed) at redshift $z = 17.2$. The black dashed line represents the same for the Λ CDM case in each figure.

fall with increasing λ . Therefore, although the allowed range of λ for Model I is $\lambda < -2\omega\Omega_\chi$ (see Table I), we limit this range to $0 < \lambda < 0.25$ for the current work.

Incorporating the above mentioned modifications in the density parameters and hence

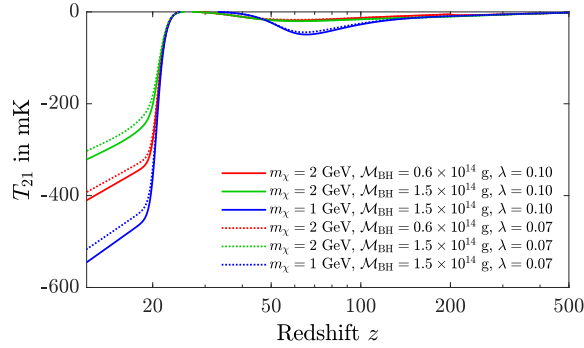


FIG. 4. Brightness temperature (T_{21}) vs redshift (z) graph for different values of DM mass (m_χ), PBH mass (\mathcal{M}_{BH}) and IDE coupling parameter λ for Model I.

the Hubble parameter, the brightness temperature of 21cm hydrogen spectra is addressed in presence of the PBH and the baryon - Dark matter interaction. In Fig. 4, we plot the brightness temperatures (T_{21}) for different values of IDE coupling parameter ($\lambda=0.07$ and 0.10) for Dark Matter masses $m_\chi=2$ and 1 GeV and PBH masses $\mathcal{M}_{\text{BH}} = 0.6 \times 10^{14}$ g and 1.5×10^{14} g while keeping β_{BH} and σ_{41} fixed at 10^{-29} and 3 respectively in the case of IDE Model I. From this figure (Fig. 4), it can be noticed that, besides DM mass and PBH mass, IDE coupling parameter λ also modifies the brightness temperature remarkably. The variation due to σ_{41} is not described in figure. However, a detail study for the variation due to σ_{41} has been carried out in Fig. 5.

In order to estimate the allowed range of the Dark Matter mass m_χ and σ_{41} , that satisfy the EDGES result for T_{21} , we give a contour plot (Fig. 5) in the $m_\chi - \sigma_{41}$ parameter space. The contour plot is generated keeping the value of z fixed at $z = 17.2$. In what follows the brightness temperature at $z = 17.2$ is represented by ΔT_{21} unless otherwise mentioned. The EDGES limit of the brightness temperature (T_{21}) at $\sim z = 17.2$ lie within the range of $-300 \text{ mK} \geq T_{21} \geq -1000 \text{ mK}$. In the current analysis, we estimate the limit for m_χ and σ_{41} using the above mentioned constraint ($-300 \text{ mK} \geq T_{21} \geq -1000 \text{ mK}$). In Fig. 5a, the calculated limiting zone for ΛCDM model (in absence of PBHs and DM - DE interaction) is plotted in the $m_\chi - \sigma_{41}$ plane using the colour code, where the individual colours indicate the different values of ΔT_{21} (colour code is described in the corresponding color-bar). This may be mentioned that the limits on m_χ obtained from these contour plots agrees with a

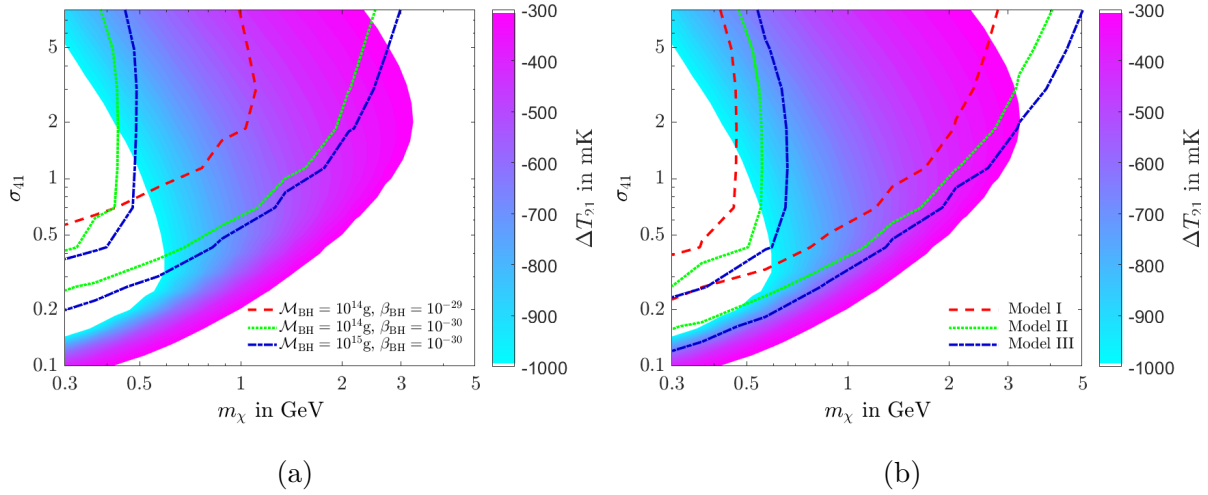


FIG. 5. The allowed region of the 21cm brightness temperature in m_χ - σ_{41} space. The coloured region represents the allowed region for the case of Λ CDM model in both the cases. In this coloured region, DM - DE interaction has not been considered. The coloured lines are representing the similar bounds for different values of PBH parameters in Fig. 5a, for the case of Model I whereas, in Fig. 5b, the estimated bounds are shown for different IDE models (at $\mathcal{M}_{\text{BH}} = 10^{14}\text{g}$, $\beta_{\text{BH}} = 10^{-30}$ and $\lambda = 0.1$)

similar calculation given in Barkana [39] (i.e. $m_\chi \leq 3 \text{ GeV}$). In both the plots (a) and (b) of Fig. 5, the coloured contour plots are generated by varying m_χ and σ_{41} and computing ΔT_{21} . We mention here that, the colour contour plots (same for Fig. 5a and 5b) are generated without considering any effects of DM - DE interaction and the PBH evaporation. Only the baryon - Dark Matter is considered and the relevant coupled differential parameters are simultaneously solved numerically, also indicated on the coloured contour plots (in m_χ - σ_{41} plane) in both Fig. 5a and 5b. The allowed regions are bound by different pairs of lines in m_χ - σ_{41} plane, when the effects of PBH or DM - DE interactions are also included. For example in Fig. 5a, the effect on the allowed region is also shown for inclusion of PBH evaporation in included with DM - DE interaction. In Fig. 5a, the PBH effect on allowed region is shown for three sets of \mathcal{M}_{BH} and β_{BH} namely $(10^{14} \text{ g}, 10^{-29})$, $(10^{14} \text{ g}, 10^{-30})$ and $(10^{15} \text{ g}, 10^{-30})$. For all these cases DM - DE interaction is also included and only Model I for DM - DE interaction is chosen ($\lambda = 0.1$). From Fig. 5a it can be seen that the region enclosed by blue dashed line corresponds to the m_χ - σ_{41} allowed region when PBH mass of 10^{14} g ($\beta_{\text{BH}} = 10^{-30}$) is chosen with Model I for DM - DE interaction. Similarly region enclosed

by the red dotted lines specify the allowed region when $\mathcal{M}_{\text{BH}} = 10^{14}$ g is considered. For the case when $\mathcal{M}_{\text{BH}} = 10^{15}$ g, $\beta_{\text{BH}} = 10^{-29}$ however, we have the left of the red dashed line is allowed. In Fig. 5b, similar regions shown to the enclosed by line plots can be identified for different IDE models namely Model I, Model II and Model III considered in this work. In Fig. 5b the PBH effect is included for $\mathcal{M}_{\text{BH}} = 10^{14}$ g and $\beta_{\text{BH}} = 10^{-29}$. From this Fig. 5, one can see that as the heating in the form of Hawking radiation increases (either for lower mass of PBH or higher initial mass fraction of PBHs) the allowed region in the m_χ - σ_{41} space shifts toward higher values of σ_{41} but lower in m_χ . In contrast, the for different IDE models, the allowed zone increases remarkably. As a consequence, the higher values of m_χ in 21cm signal seems to indicate the effect of DM-DE interaction.

Finally, a detailed study has been carried out to explore similar bounds in the \mathcal{M}_{BH} - λ plane for individual IDE models with dark matter mass $m_\chi = 0.5$ GeV, 1.0 GeV and 1.5 GeV. In each of the cases, the value of σ_{41} is set to 1.0. These are shown in Fig. 6, The first, second and third row correspond to the IDE Model I, II and III respectively. Fig. 6a shows the fluctuation of ΔT_{21} in \mathcal{M}_{BH} - λ space for $m_\chi = 0.5$ GeV and the IDE Model I with $\lambda = 0.1$, where the value of ΔT_{21} at each point is described in the colour bar place at the end of the row. In all the plots in Fig. 6, the yellow dashed line represents the bounds from EDGES result. Fig. 6b and Fig. 6c describe the same for $m_\chi = 1.0$ GeV and 1.5 GeV respectively. From these figures (Fig. 6a, 6b and 6c) it can be seen that, as \mathcal{M}_{BH} increases, the numerical value of ΔT_{21} decreases for any particular value of λ (except a little distortion at $\mathcal{M}_{\text{BH}} = 1.7 \times 10^{14}$ g and $\lambda < 0.08$). Simultaneously, with increasing m_χ , ΔT_{21} also increases. We repeat our calculation for Model II and Model III also and the results are furnished in Fig. 6d, 6e, 6f and Fig. 6g, 6h, 6i respectively. From these figures (all plots of Fig. 6), it can be noticed that, for $m_\chi = 0.5$ GeV, the IDE model constraints (see benchmark points described in Table II) satisfy the EDGES limit in each IDE models. Those constraints are also agree with the EDGES limit for $\mathcal{M}_{\text{BH}} \lesssim 1.5 \times 10^{14}$ g and $\mathcal{M}_{\text{BH}} \gtrsim 1.8 \times 10^{14}$ g, when $m_\chi = 1.0$ is considered. But, in the case of higher values of m_χ (for example $m_\chi = 1.5$ GeV, see Fig. 5c, Fig. 5f and Fig. 5i) the IDE constraints do not satisfy, although the allowed region exists in the stability limit as described in Table I for all IDE models.

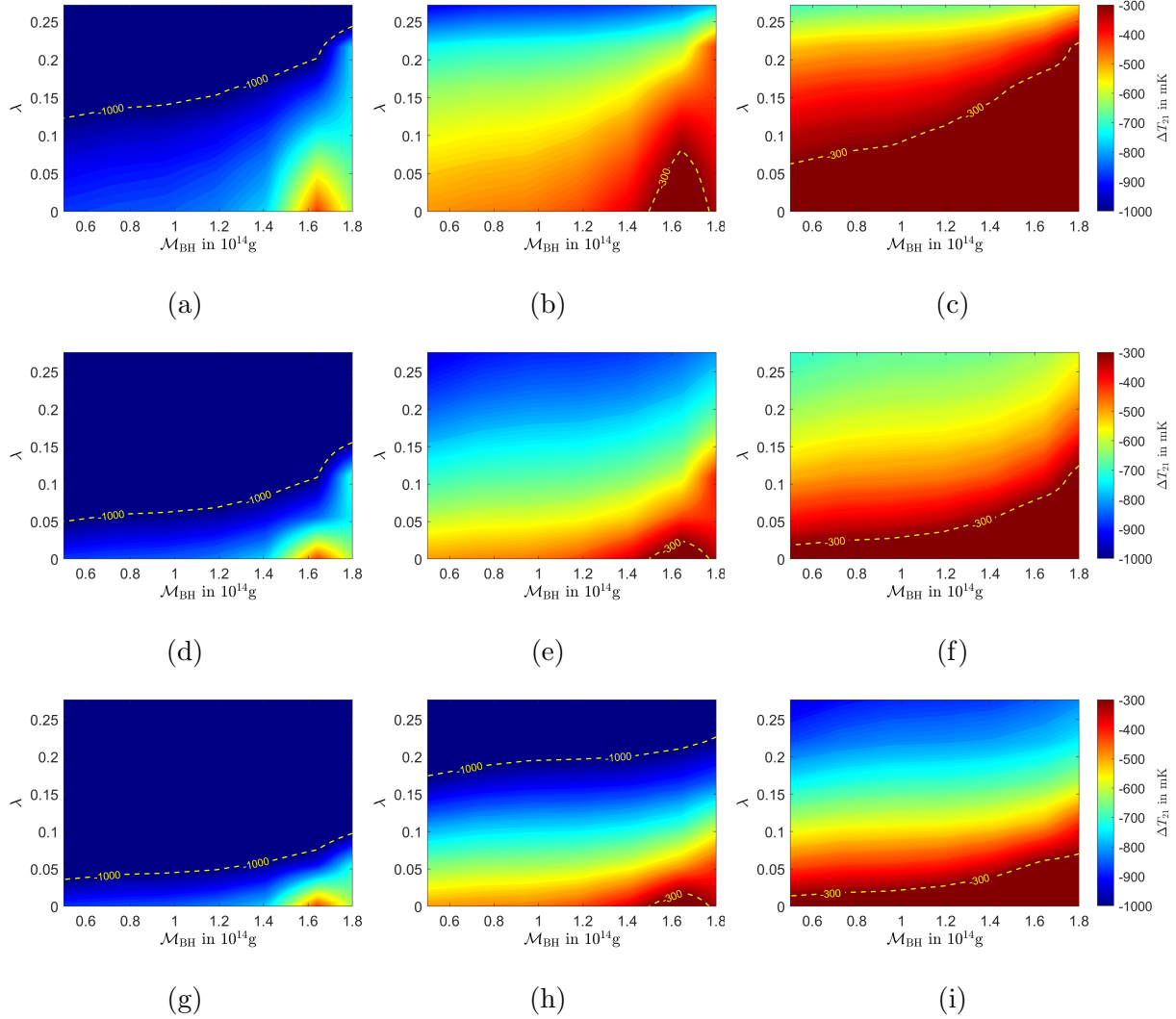


FIG. 6. Variation of ΔT_{21} with PBH mass and DE-DM coupling parameter λ for different DM masses and IDE models (see Section II).

VII. SUMMARY AND DISCUSSIONS

In this work we have studied the upper-bound of DM-DE interaction coupling (λ) for different values of PBH masses (\mathcal{M}_{BH}) in the context of DM-DE interaction. The DM-DE interaction modifies the Hubble parameter $H(z)$ and hence the optical depth of the ISM along with the thermal evolution of the Universe. As a consequence, the brightness temperature of 21cm line T_{21} also shows significant variation with λ (see Fig. 4 and Fig. 6). In the current work, we evolve the coupled parameters ρ_χ , ρ_{de} , \mathcal{M}_{BH} , T_b , T_χ , x_e and $V_{\chi b}$ (Eqs. 1, 2, 3, 8, 9, 10 and 17) simultaneously with redshift z to explore the variation of brightness temperature (T_{21}) with different parameters. The effect of baryon-DM interaction

shows significant modification in thermal evolution. In Fig. 1, 2 and 4, the fluctuations in brightness temperature are shown. The modification of the Hubble evolution with model parameters are also shown in detail in Fig. 3). Eventually we investigate the bounds for the parameters used in the current work, that satisfy the constraints proposed by EDGES.

The entire calculations are carried out in the framework of three IDE models (Dark Matter - Dark Energy interaction), governed by interaction coupling parameter λ keeping the stability limits described in Table I. From the analysis of Fig. 6 one can conclude that, the model constraints described in Table II [16–23] satisfy the EDGES limit at lower masses of dark matter (≤ 1.0 GeV) for the IDE models. However, those does not agree with the same for $m_\chi \gtrsim 1$ GeV (for each three IDE models). Hopefully, future investigation related to 21cm physics will enrich our understanding about the thermal evolution and dynamics of the early Universe.

ACKNOWLEDGEMENTS

One of the authors (A.H.) wish to acknowledge the support received from St. Xavier’s College, Kolkata and the University Grant Commission (UGC) of the Government of India, for providing financial support, in the form of UGC-CSIR NET-JRF. One of the authors (MP) thanks the DST-INSPIRE fellowship (DST/INSPIRE/FELLOWSHIP/IF160004) grant by DST, Govt. of India.

-
- [1] J. D. Bowman, A. E. E. Rogers, R. A. Monsalve, T. J. Mozdzen, and N. Mahesh, *Nature* **555**, 67 (2018).
 - [2] M. Y. Khlopov, *Research in Astronomy and Astrophysics* **10**, 495 (2010).
 - [3] K. M. Belotsky, A. E. Dmitriev, E. A. Esipova, V. A. Gani, A. V. Grobov, M. Y. Khlopov, A. A. Kirillov, S. G. Rubin, and I. V. Svadkovsky, *Modern Physics Letters A* **29**, 1440005 (2014).
 - [4] K. M. Belotsky, V. I. Dokuchaev, Y. N. Eroshenko, E. A. Esipova, M. Y. Khlopov, L. A. Khromykh, A. A. Kirillov, V. V. Nikulin, S. G. Rubin, and I. V. Svadkovsky, *The European Physical Journal C* **79**, 246 (2019).

- [5] J. García-Bellido, Journal of Physics: Conference Series **840**, 012032 (2017).
- [6] S. J. Clark, B. Dutta, Y. Gao, Y.-Z. Ma, and L. E. Strigari, Phys. Rev. D **98**, 043006 (2018).
- [7] Y. Yang, Phys. Rev. D **102**, 083538 (2020).
- [8] O. Mena, S. Palomares-Ruiz, P. Villanueva-Domingo, and S. J. Witte, Phys. Rev. D **100**, 043540 (2019).
- [9] K. J. Mack and D. H. Wesley, “Primordial black holes in the dark ages: Observational prospects for future 21cm surveys,” (2008), arXiv:0805.1531 [astro-ph].
- [10] K. L. Pandey and A. Mangalam, Journal of Astrophysics and Astronomy **39**, 9 (2018).
- [11] J. B. Muñoz, E. D. Kovetz, and Y. Ali-Haïmoud, Phys. Rev. D **92**, 083528 (2015).
- [12] C. Li, X. Ren, M. Khurshudyan, and Y.-F. Cai, Physics Letters B **801**, 135141 (2020).
- [13] U. Mukhopadhyay, D. Majumdar, and K. K. Datta, (2020), arXiv:2008.09972 [astro-ph.CO].
- [14] Z.-K. Guo, N. Ohta, and S. Tsujikawa, Phys. Rev. D **76**, 023508 (2007).
- [15] E. Di Valentino, A. Melchiorri, O. Mena, and S. Vagnozzi, Phys. Rev. D **101**, 063502 (2020).
- [16] A. A. Costa, X.-D. Xu, B. Wang, and E. Abdalla, Journal of Cosmology and Astroparticle Physics **2017**, 028 (2017).
- [17] O. Bertolami, F. Gil Pedro, and M. Le Delliou, Physics Letters B **654**, 165 (2007).
- [18] J.-H. He, B. Wang, and E. Abdalla, Phys. Rev. D **83**, 063515 (2011).
- [19] L. Santos, W. Zhao, E. G. M. Ferreira, and J. Quintin, Phys. Rev. D **96**, 103529 (2017).
- [20] W. Yang, S. Pan, and A. Paliathanasis, Monthly Notices of the Royal Astronomical Society **482**, 1007 (2018).
- [21] M. Le Delliou, R. J. F. Marcondes, and G. B. Lima Neto, Monthly Notices of the Royal Astronomical Society **490**, 1944 (2019).
- [22] M. Gavela, D. Hernández, L. L. Honorez, O. Mena, and S. Rigolin, Journal of Cosmology and Astroparticle Physics **2009**, 034 (2009).
- [23] J.-H. He, B. Wang, and E. Abdalla, Physics Letters B **671**, 139 (2009).
- [24] J. H. MacGibbon, Phys. Rev. D **44**, 376 (1991).
- [25] S. Galli, T. R. Slatyer, M. Valdes, and F. Iocco, Phys. Rev. D **88**, 063502 (2013).
- [26] P. J. E. Peebles, Astrophysical Journal **153**, 1 (1968).
- [27] Y. Ali-Haïmoud and C. M. Hirata, Phys. Rev. D **83**, 043513 (2011).
- [28] D. Pequignot, P. Petitjean, and C. Boisson, A&A **251**, 680 (1991).
- [29] D. G. Hummer, MNRAS **268**, 109 (1994).

- [30] S. Seager, D. D. Sasselov, and D. Scott, *The Astrophysical Journal* **523**, L1 (1999).
- [31] B. J. Carr, K. Kohri, Y. Sendouda, and J. Yokoyama, *Phys. Rev. D* **81**, 104019 (2010).
- [32] X. Chen and M. Kamionkowski, *Phys. Rev. D* **70**, 043502 (2004).
- [33] Y. Ali-Haïmoud and C. M. Hirata, *Phys. Rev. D* **82**, 063521 (2010).
- [34] Q. Yuan, B. Yue, X.-J. Bi, X. Chen, and X. Zhang, *Journal of Cosmology and Astroparticle Physics* **2010**, 023 (2010).
- [35] M. Kuhlen, P. Madau, and R. Montgomery, *The Astrophysical Journal* **637**, L1 (2006).
- [36] W. Yang, S. Pan, S. Vagnozzi, E. D. Valentino, D. F. Mota, and S. Capozziello, *Journal of Cosmology and Astroparticle Physics* **2019**, 044 (2019).
- [37] C. M. Hirata, *Monthly Notices of the Royal Astronomical Society* **367**, 259 (2006).
- [38] B. Ciardi and P. Madau, *The Astrophysical Journal* **596**, 1 (2003).
- [39] R. Barkana, *Nature* **555**, 71 (2018).